River bank instability from unsustainable sand mining in the lower Mekong River

Christopher R. Hackney[1]*, Stephen E. Darby[2], Daniel R. Parsons[1], Julian Leyland[2], James L. Best[3], Rolf Aalto[4], Andrew P. Nicholas[4] and Robert C. Houseago[1].

[1]Energy and Environment Institute, University of Hull, Hull, HU6 7RX, UK

[2]School of Geography and Environmental Sciences, University of Southampton, Southampton, SO17 1BJ, UK.

[3]Departments of Geology, Geography and GIS, Mechanical Science and Engineering and Ven Te Chow Hydrosystems Laboratory, University of Illinois at Urbana-Champaign, Urbana, IL 61801, USA.

[4]College of Life and Environmental Sciences, University of Exeter, Exeter, EX4 4RJ, UK.

**Corresponding author email address: c.hackney@hull.ac.uk; (https://orcid.org/0000-0001-5390-9136)*

Recent growth of the construction industry has fuelled demand for sand, with considerable volumes being extracted from the world's large rivers. Sediment transport from upstream naturally replenishes sediment stored in river beds, but the absence of sand flux data from large rivers inhibits assessment of the sustainability of ongoing sand mining. Here, we demonstrate that bedload (0.18 Mt yr^{-1} ± 0.07 Mt yr^{-1}) is a small (1%) fraction of the total annual sediment load of the lower Mekong River. Even when considering suspended sand (6 Mt yr^{-1} ± 2 Mt), the total sand flux entering the Mekong delta (6.18 Mt yr^{-1} ± 2.01 Mt yr^{-1}) is far less than current sand extraction rates (50 Mt yr^{-1}). We show that at

these current rates, river bed levels can be lowered sufficiently to induce river bank instability, potentially damaging housing, infrastructure and threatening lives. Our research suggests that, on the Mekong and other large rivers subject to excessive sand mining, it is imperative to establish regulatory frameworks that limit extraction rates to levels that permit the establishment of a sustainable balance between the natural supply/storage of sand and the rate at which sand is removed.

The world is currently undergoing rapid population growth, urbanisation and, in some regions, economic development. Between 1950 and 2018, urban populations increased from 751 million to 4.2 billion people[1] , and by 2050 it is estimated that 68% of the world's population will reside in cities, with Africa and Asia seeing the vast majority (90%) of this growth[1]. As a result, concrete production across the globe has grown appreciably, from 2,000 Mt yr^{-1} in 1950[(Ref. 2)] to > 30,000 Mt yr^{-1} today[3], fuelling major demand for aggregate resources[4–6]. Additionally, vast quantities of sand are used in land reclamation programmes around the world. Along with the coastal zone, many of the world's large sand-bedded rivers provide a readily available source of construction-grade sand[7–9]. At a global scale, current rates of sand mining from both coasts and rivers (~40,000 Mt yr^{-1})[4] significantly outstrip estimates of total global fluvial sediment discharge (19,000 Mt yr^{-1})[10]. However, we currently lack reliable estimates of fluvial sand fluxes, especially for the portion of sand flux transported as bedload. Quantifying bedload transport rates is vital as it is the stores of sand on the river bed that are often exploited, rather than sand transported in suspension. We also lack robust knowledge of sand mining and sand extraction rates from rivers. These data gaps arise from the fact that much sand mining activity is unregulated and unmonitored, and because there is a lack of

sediment transport data from many large rivers[8]. This lack of knowledge means that it is not possible to assess reliably the extent to which exploitation of riverine sand reserves is, or is not, outpacing the natural replenishment of sand by transport from upstream.

The Mekong River is one of the world's largest sand-bedded rivers (along with the Ganges-Brahmaputra, Irrawaddy, Salween, Changjiang and Huang He rivers) that drain the Tibetan Plateau[8]. The Mekong delivers significant quantities of water (450 $km^3\ yr^{-1}$)[11] and suspended sediment (87 Mt yr^{-1})[12] to the South China Sea. As with many major river deltas, the Mekong delta has witnessed increasing economic development in recent decades, at the same time as concerns that reductions in fluvial sediment supply may be compounding the threat of rising sea-level[8-17]. Recent estimates of the suspended sediment load of the alluvial reaches of the Lower Mekong River downstream of Kratie, Cambodia (henceforth referred to as the LMR) (~87 Mt yr^{-1}; ref [12]) suggest that sediment loads have declined substantially over recent decades from their historical levels of ~160 Mt yr^{-1}, in part due to changes in climate and anthropogenic activities[12–15]. In particular, the expansive development of hydropower throughout the Mekong River basin is projected to result in the trapping of a large proportion (up to 96%)[8,16] of the alluvial sediment load[19–21] and flow regulation has also altered the natural monsoon-driven hydrological cycle, reducing the flood peaks that typically transport the largest sediment loads[14,19–21].

There are also uncertainties regarding how much sand is being extracted from the LMR. One study[22] has suggested that approximately 34 Mm^3 (55 Mt yr^{-1}) of aggregate is being extracted annually, of which 90% (31 Mm^3 or 50 Mt yr^{-1}) is sand (with the remaining 10% being coarser, i.e. gravel), with more than 80% of this sediment being mined from the alluvial reaches of the LMR in Cambodia and

Vietnam[22] (Fig. 1a). This estimate was derived from questionnaire data collected at mining sites in four countries in the Mekong River basin (Lao PDR, Thailand, Cambodia and Vietnam) during low flow conditions in 2011 and 2012. However, in the subsequent seven years since this study, demand for sand has increased considerably, hence the commonly reported value of sediment extraction based on the 2011-2012 data is likely now to be lower than actual current extraction rates. Mining practices frequently target sediment from stores of sand (bedforms) on the river bed[22,23]. The removal of sand has been shown to alter the riverbed morphology, reduce flow velocities and increase flow turbulence around the mining pit areas[23,24], sometimes with undesirable impacts. For example, there has been speculation that perceived increases in rates of bank erosion are caused by sand mining[8,14,23 - 26]. However, with large uncertainties in estimates of both the river sand flux and sand extraction rates, detailed quantitative assessments, both of the extent to which the rate of sand mining is, or is not, sustainable, and of the impacts of sand mining on bank erosion, remain absent. Here, we provide the first quantification of bedload transport rates on the LMR and use these data, together with estimates of the suspended sand load, to compute the total sand flux being transported to the apex of the Mekong delta. By comparing with current rates of sand mining and by estimating the volume of sand stored in the bed substrate of the LMR, we provide the first comprehensive overview of the extent to which current rates of sand extraction are unsustainable. We show that excessive sand mining is inducing river bed lowering that in turn leads to the onset of river bank instability, raising the likelihood of dangerous river bank collapse in locations where mining operations are present.

Bedload sediment transport in the Lower Mekong River

If undertaken at all, the extraction of river bed sand should be conducted at rates that are less than the rate at which sand is redeposited from either bedload or suspended load transported from upstream. Downstream of Kratie, Cambodia, sand grade sediment in suspension is known to comprise only *c.* 7% of the total suspended load (Fig. 1b), but it is poorly known how much sand is transported as bedload. However, bedload transport rates of large rivers such as the Mekong have in the past been very difficult to measure due to their great depths (often > 25 m) and the dynamic conditions at the water-bed interface[27]. Bedload transport is also highest during the largest flow discharges, making data collection difficult and dangerous. Existing estimates suggest that large-river bedload fluxes may vary in the range of 20 – 30% of the total load, for the suspended concentrations observed on the LMR[28]. Yet, the sole existing estimate of bedload transport in the alluvial reaches of the LMR in Cambodia suggests that the contemporary bedload flux may be much smaller; ~1.5% of the suspended sediment load[16]. This existing bedload transport estimate was based on point-samples collected at one site (Kratie) in one year (2011)[17,29]. Here, we provide new estimates of bedload transport derived from repeat bathymetric surveys (see Methods for how these estimates were derived) undertaken across six sites (Fig. 1b) throughout the LMR in Cambodia between 2013 and 2014 and covering a wide range of flows (14,000 $m^3 s^{-1}$ to 55,000 $m^3 s^{-1}$).

We use the bedload estimates obtained from these repeat bathymetric surveys, alongside measurements of flow conditions and bed material characteristics (see Methods), to construct a physically meaningful bedload transport function (Fig. 2a) in which instantaneous bedload transport rates per unit width (kg s^{-1} m^{-1}) are plotted as a function of excess unit stream power following the approach of Bagnold[30] (see Methods). The unit fluxes so computed are also integrated across the channel width

to assess the fraction of the total sediment flux that is composed of bedload and suspended load (the calculation of the latter is described in the Methods) (Fig. 2b). We then also estimate annual bedload transport rates by integrating the bedload transport function (Fig. 2a) across the time period 1981 – 2014, using flow discharge data from the Kratie gauging station (*see* Methods and Supplementary Figure S1). The proportion of sand is then estimated based on observed grain size distributions of the bed material (bedload) and suspended sediment (*see* Methods and Table S2).

Over the period 1981 – 2014, annual bedload transport is estimated to be, on average, 0.18 ± 0.07 Mt yr^{-1}, which is < 1% (0.2%) of the suspended load at Kratie (87.4 ± 28.7 Mt yr^{-1} during the same period[12]). Across the course of the annual monsoonal flood hydrograph, the percentage of sediment flux that is transported as bedload varies from 0.05% to 1.5% (Fig. 2b). This low percentage of bedload is in agreement with the previous estimate of bedload at Kratie that places bedload at 1.5% of the total sediment load[17,29]. Sediment fluxes predicted from reliable bedform tracking presented for the LMR herein highlight that there is less sediment than previously thought available to replenish stores of sediment removed through mining activities. Our surveys cover a wide range of flows (14,000 $m^3 s^{-1}$ to 55,000 $m^3 s^{-1}$, compared to the mean peak discharge at Kratie of 36,700 $m^3 s^{-1}$ for the period 1960 – 2004[11]) that transport a large majority (78%) of all bedload during the period 1981 - 2014 (Fig. 2c). We emphasise that although our surveys only cover a one year period and omit flows lower than 14,000 $m^3 s^{-1}$ (accounting for 19% of total bedload between 1981 and 2014) and flows higher than 55,000 $m^3 s^{-1}$ (accounting for 3% of total bedload between 1981 and 2014) our data captures a high range of variability in bedload transport rates and thus represent much of the observed long term natural variability in bedload (Fig. 2c).

Supply, stores and extraction of sediment

The available sand resource (S_{res}) in the bed of the LMR can be conceptualised as a balance between the incoming supply of sand, S_{in} (Mt yr^{-1}), the rate of sand extraction, S_{xt} (Mt yr^{-1}) over a given number of years (t) and the available mass of sand in storage, S_{store}, in the bed (Mt) such that:

$$S_{res} = S_{store} + ((S_{in} - S_{xt}) * t) \quad (3)$$

The key components of Eq. 3 concerning the sustainability of the sand resource relate to the balance between the incoming sediment load (S_{in}) and the rate of sand extraction (S_{xt}). Using our estimates of sand transport detailed above, we are able to provide estimates of S_{in}, which comprises the sum of the sand being transported as bedload (0.18 ± 0.07 Mt yr^{-1}) and that transported in suspension, which is 7% of the total suspended sediment load of the LMR (6 Mt yr^{-1} ± 2 Mt yr^{-1}; Fig. 1b). Thus, S_{in} equates to 6.18 Mt yr^{-1} (± 2.07 Mt yr^{-1}). Recent work has revealed that the total suspended sediment load at Kratie has been declining by ~2 Mt yr^{-1} (Ref. 12). As the suspended load comprises >93% of the total sand load, it follows that the magnitude of S_{in}, and therefore the total amount of sand being transported downstream of Kratie, has also been in decline over the past few decades.

Between 2001 and 2011, the number of mining operations active on the LMR rose from 15 to 70 (Ref. 25). Therefore, over this period, the magnitude of S_{xt} is likely to have increased, although no data to quantify this increase has been reported. In 2011 S_{xt} was estimated to be *c*. 50 Mt yr^{-1} (Ref. 22), yet recent studies have refined this estimate by assuming a variation of 25% around the central estimate of 50 Mt yr^{-1} to account for subsequent changes in the years following the study[18]. Here, we assume similar

bounds and provide an upper and lower estimate of S_{xt} following Koehnkhen[21] of 37 to 62 Mt yr^{-1}, respectively, with values for the upper and lower bounds henceforth reported in parentheses.

We note here that we do not account for exchanges between the river and the expansive floodplains south of Kratie. Although sediment is deposited onto the floodplains during the monsoon season[31,32], the amount of sand sequestered is currently unquantified. That said, we have shown above that the suspended load of the Mekong is predominantly fine silts and clays (Fig. 1b) and given that the sand fraction will predominantly be transported close to the river bed, we would expect the majority of overbank sediment dispersal to be associated with the finer fractions.

The value of S_{store} represents the depth of the alluvial deposits of sand that comprise the channel bed of the LMR. The area of active channel (defined as the bankfull channel area of the Mekong River) between Kratie and the South China Sea, including the Bassac and delta distributary channels, is ~1,600 km^2. Data from boreholes, cores, resistivity and seismic surveys through Cambodia and Vietnam show that the thickness of sand under the channel varies spatially across the alluvial reaches of the Mekong[33–39]; from 45 m near Kampong Cham[35] to 25 m south of Phnom Penh[39] (*see* Supplementary Information). On average, the thickness of alluvial deposits in and around the LMR channel is 28 m. Thus, as a first approximation, when combined with the total area of channel, S_{store} has a value of 71,098 Mt (assuming a sand density of 1,600 kg m^{-3}). Although seemingly extensive, we note that this value may provide a false representation of the risks associated with sediment extraction as it neglects to account for the sensitivity of the river system to the rate of extraction.

The current balance of sand supply to extraction results in a 44 Mt yr^{-1} (31 Mt yr^{-1} and 56 Mt yr^{-1}) deficit in the sand budget of the LMR, with seven (between five and nine) times the natural supply of sand being removed by mining activities annually. Such a large deficit between the input of sand from upstream and its removal by mining activities means that river bed incision is an inevitable consequence of the current high rates of sand extraction. The precise rate of this incision will vary spatially in relation to the local intensity of sand mining operations, but recent studies have reported that rates of incision in the downstream portion of the Mekong delta are of the order of 0.13 m yr^{-1} (Ref 23). This demonstrates the clear impact that sand extraction can have on channel morphology, local hydrodynamics[23,26], and hence local channel stability, with attendant consequences for infrastructure stability (e.g. loss of housing, road networks and undermining bridge piers and foundations) and wildlife habitat and agricultural land provision. The impacts of sand mining on bed level lowering can be clearly seen in the bathymetry of impacted reaches of the LMR (Fig. 3a) where a pockmarked surface depicts the locations of extraction activities. Individual pockmarks measure up to 70 m in diameter and 10 m in depth (Fig. 3b). Over the 0.67 km^2 area affected by mining activities highlighted in Fig. 3a, a total of 559 individual pockmarks can be identified. This equates to a total volume of sand extracted of *c*. 2,748,023 m^3 (1.03 Mt; assuming pits are typically hemispherical and a sediment density of 1,600 kg m^{-3}). The cumulative impact of mining over a ten year period along a 25 km reach of the Bassac River, one of the Mekong delta's main distributary channels, has been shown to induce channel incision of up to 0.59 m yr^{-1} in the Mekong delta[23]. Thus, given the apparent propensity of mining operations throughout the LMR, extraction is likely to be resulting in significant channel incision across the LMR along with substantial coastal land loss[15,18].

Although past studies have speculated that mining induced channel incision has the potential to cause marked increases in bank erosion rates[23], the impact on bank stability of a reduction in river bed levels due to mining has not previously been quantified. Using 19 bank profiles collated from terrestrial laser scanning and MBES data (*see* Methods) along a 25 km stretch of the LMR (Fig. 1a), we quantify the stability of the river banks (Fig. 4) for a range of likely channel incision scenarios (bed lowering ranging from one to six meters) based on the depths of mining observed in Fig. 3b (see Methods for details). Our results clearly show how even modest levels of bed scour (*c.* 2 m) can cause entire sections of river banks along the LMR to shift from a stable state to a condition where they become seasonally unstable (i.e., they are liable to failure when the banks become saturated during the monsoon flood; Fig. 4b). At the maximum 6 m lowering investigated herein, the majority (63%) of river profiles studied fall into the seasonally unstable category. Previous work[23] has suggested that in the period 1998 – 2008 mining induced incision rates in the Mekong delta were, locally, of the order 0.5 m yr^{-1} . As such, the Mekong system may be already well on its way towards system wide instability of its river banks. A clear distinction between vegetated and unvegetated banks is also demonstrated (Fig. 4), with vegetated banks proving more resistant to mining induced toe-scour. Specifically, only 20% of vegetated banks become seasonally unstable as a result of bed level lowering, and only at the maximum 6 m change. This is compared to the majority of unvegetated banks (57%) becoming seasonally unstable with a 3 m lowering (Fig. 4b). As shown in Figure 3b, two to three meters is the modal value of mining pit depths observed. It is acknowledged that vegetation is more likely to be present on lower angled banks due to the preference of vegetation

to colonise less steep banks, thus providing an additional source of cohesion to the bank material. However, our results indicate that bank re-profiling to make banks shallower in angle, as well as promoting re-vegetation, might provide an affordable means of diminishing the susceptibility of river banks to potential collapse.

Discussion

Our work highlights the need for more sustainable, evidence-based, management practices and plans regarding the extraction of river sediment. For example, we show above that incision of the river bed can increase bank height and induce instability, threatening key infrastructure and communities located on the banks of the river. One way to reduce the potential of sand mining to induce bank instability would be to confine sand extraction only to the middle of the channel, away from river banks, although this will just delay the impact rather than halt it. Additionally, sand mining should be regulated to take account of local patterns of sediment accumulation and deficit. For example it may be possible to adopt more sustainable extraction practices by targeting mining on those local areas of the channel where sediment is accumulating rapidly, such as on major channel bars.

The role that the sediment load of the LMR plays in the socio-economic sustainability of the Mekong River basin has long been appreciated, and recent projections highlight both the likelihood of increased sediment retention in hydropower reservoirs in the LMR catchment[16,19] and natural reductions in sediment load caused by changes to the regional patterns of cyclone-related preciptation[11]. Reduced fluvial inputs of sand will thus exacerbate the impact of maintained, or even increased, levels of sand extraction into the future. In a transboundary catchment such as the

Mekong, these factors will also act to exacerbate the threat posed by the negative sand balance identified herein[8] across national boundaries. Sediment extraction in Cambodia, for example, has the potential to impact flood risk and environmental resilience in the Vietnamese part of the Mekong delta. As such sustainable management plans need to focus not only on the local-, but also the basin-scale impacts of sand mining. Left unaddressed, it is likely that increased channel and infrastructure instability, greater coastal erosion and magnified flood risk may result from an increased deficit in sand supply[15,18,23] and that the hydrodynamic and morphological processes of a sediment-starved LMR will readjust to these changes in bathymetry. Although the research herein has focused on the LMR, the issue of sediment mining is pertinent to many of the world's large sand bedded rivers[8]. It is therefore imperative that regulatory frameworks are established in which local extraction levels can be monitored to permit establishment of a sustainable balance between the natural supply/store and the extracted resource of individual fluvial systems. Such monitoring and regulation are essential in order to preserve the long-term sustainability of sand resources in the world's major rivers and help assure the required delivery of sand to their deltas downstream.

Correspondence and request for material should be made to CH.

Acknowledgements

This study was supported by awards NE/JO21970/1, NE/JO21571/1 and NE/JO21881/1 from the UK Natural Environmental Research Council (NERC). We thank the Mekong River Commission for access to hydrological and suspended sediment data and the Department for Hydrology and Water Resources in Cambodia

for their logistical support and help in the field. J.L.B. was in receipt of a University of Southampton Diamond Jubilee International Visiting Fellowship that aided completion of this work.

Author Contributions

C.R.H., S.E.D., D.R.P., J.L., J.L.B., A.P.N. and R.A. jointly conceived the study. C.R.H., S.E.D., J.L., J.L.B., D.R.P., R.A and R.H. collected and processed the field data. C.R.H. constructed the bedload transport functions and undertook the data analysis. C.R.H and S.E.D. undertook the bank stability analysis. C.R.H. drafted the paper, which was then edited by all co-authors.

Competing Interests

The authors declare no competing interests.

Methods

Below we detail the methods and techniques used to capture the data presented above.

Bathymetry Data

High-resolution multibeam echo sounding (MBES) surveys were undertaken at six locations (see Table S1) between Phnom Penh and Kratie, Cambodia, during 2013 and 2014. We employed a RESON SeaBat 7125 MBES operating at 400kHz and forming 512 equal-angle beams across a 140° swath. A Leica 1230 differential global positioning system (dGPS) was used in Real Time Kinematic (RTK) mode to provide position at 1 Hz with accuracy of ±0.02m and ±0.03m in the horizontal and vertical, respectively. The dGPS was coupled to an Applanix POS-MV WaveMaster inertial motion unit (IMU), which provided full, real-time, three-dimensional (3-D) motion and heading data correction, at 100 Hz, for the MBES, along with synchronization of all survey data streams using the dGPS time stamp and a pulse per second (PPS) signal. Post-survey calibration, correction for angular offsets, and correction for temporal variation in water surface elevation, were applied to the MBES data within CARIS HIPS and SIPS (v.9) software. Extraneous data points from in the water column (false targets) and secondary bed returns, were manually removed prior to 3D surface analysis in CloudCompare (https://www.danielgm.net/cc/).

Bank Profile Data

Bank topography was generated through combined subaqueous morphology obtained from the six MBES surveys (*see* above) with sub-aerial topography captured with a vessel-mounted Leica P20 Terrestrial Laser Scanner (TLS) in July

2014. The TLS was also located spatially and temporally with the dGPS coupled to an Applaniz POS-MV WaveMaster inertial motion unit. The survey data was collected using QPS Quality Integrated Navigation System Software and post-processed in CloudCompare. Vegetation and other unwanted data were removed using the CANUPO plugin with additional manual data removal.

Bed Material Sampling

At each of the six MBES survey locations, three bed material samples were collected at 0.25, 0.5 and 0.75 of the channel width. Samples were collected with an Ekman-style grab sampler. Each sample was subsequently dry sieved for grains > 75 μm, whilst finer grains were analysed using a Saturn Digisizer to estimate the full grain size distribution of each sample (see Table S2).

Suspended Material Sampling

Suspended sediment was collected using a 2.2 L Van Dorn sampler at each site during 2013 and 2014. At each site, three samples were taken in the vertical at 0.25, 0.5 and 0.75 the water depth, and at three locations across the channel. Grain size was analysed using a Saturn Digisizer. These samples are then aggregated to a cross-section mean grain size distribution (see Table S2).

Flow monitoring and suspended sediment calculations

Detailed 3D time-mean flow velocity fields were obtained at each MBES survey location using acoustic Doppler current profilers (aDcp). Specifically, we employed

two RDI Teledyne RioGrande 600kHz and one RDI Teledyne RioGrande 1200kHz units in river depths ranging from 13.5 m to 40.1 m, depending on flow season and site (see Table S1 for flow ranges at each site). Flow measurements were made at a series of predetermined cross-sections that were located in the centre of the MBES survey areas. At each cross-section, four repeat transects were undertaken to resolve the time-averaged flow field[40]. Each aDcp unit was coupled to the same RTK dGPS used in the MBES surveys to determine the position and velocity of the survey vessel. Following Szupiany et al.[40], boat speed and trajectory were constantly monitored during the survey to reduce associated errors by ensuring that boat speed did not exceed the flow velocity. The primary and secondary flow structures (if present) at each cross-section were obtained through processing and vector rotation using the Velocity Mapping Toolbox (VMT) [41] and were defined using a zero net cross-stream discharge decomposition[42].

Cross-sectional suspended sediment concentrations (SSC) and overall sediment flux were estimated by calibrating the corrected acoustic backscatter (ABS) value recorded by the aDcp to SSC [43-45]. This relationship is based on the assumption that the intensity of the acoustic backscatter recorded by the aDcp is a function not only of equipment characteristics but also water column conditions (i.e. the concentration and size of suspended sediment therein). Therefore, for a given instrument and sediment type and sediment size distribution, a simple relationship between acoustic backscatter and SSC can be obtained[44]. The development of the calibration functions used herein are described in detail elsewhere[11,29]. In summary, we collected point water samples using a 2.2 L Van Dorn (Rutner) sampler at three evenly spaced verticals across the channel and at three points within each vertical profile. These point water samples were obtained across a variety of flow conditions

and locations; the samples were then analysed for SSC by filtering (Whatman GF/C glass microfibre grade, 47 mm diameter, 1.2 μm filter paper) and weighing the dry mass of solids retained from the water samples. The range of SSC covered by this sampling procedure was 6–531 mg L^{-1}. Simultaneous aDcp measurements were taken to enable comparison between the directly measured suspended sediment concentrations and the recorded acoustic backscatter such that we were able to produce unique SSC versus ABS calibration curves for each of the three aDcp units employed in this study[11,29]. The resultant calibration curves display strong correlations that are significant at 95% confidence levels (with r^2 values of 0.83, 0.87 and 0.67, for the two 600kHz units and the 1200kHz unit, respectively). For each cross-section, the acoustic backscatter values were converted to a SSC using the appropriate calibration curve. The associated flow velocity measurements from the aDcp were then used to convert these concentrations into a sediment mass flux at each cell, and finally these were integrated across each cross-section to provide an instantaneous section-averaged suspended sediment load (kg s^{-1}).

Bedload transport estimates

At each of the six MBES survey sites, we subdivided the channel into a series of cross-channel subsections (n = 5) based on changes in bedform morphology, dune type and channel location (i.e. outside of a meander bend vs inside of a meander bend). This was done to account for spatial variations in sediment transport across the channel width. We note that bedload transport is likely to vary spatially, hence why we have captured data from nine locations in Cambodia. However, it is acknowledged that other parts of the Mekong basin may have markedly different

bedload transport rates. Additional research and data is needed, therefore, to build up a complete picture of bedload transport across the entire Mekong basin.

Following past work[27], channel-width integrated sediment transport rates (Q_b; kg s^{-1} m^{-1}) were then calculated by averaging the instantaneous fluxes (q_b) in each sub-section and integrating the average rate per unit width out across the channel width. Within each sub-section, instantaneous transport rates per unit width were estimated by calculating the downstream translation distance (Δx; m) of a dune form between repeat MBES surveys over a given time, Δt, such that:

$$\langle \Delta X \rangle = \frac{\sum area[Z(t_2) < Z(t_1)]}{N_{bedform}\, X\, W_{dune}} \quad (1)$$

where $Z(t_1)$ is the bed elevation at time 1 and $Z(t_2)$ is the bed elevation at time 2, $N_{bedform}$ is the number of bedforms in the defined reach and W_{dune} is the effective width of the survey panel. The sub-section instantaneous fluxes per unit width (q_b; *kg* s^{-1} m^{-1}) were then defined as:

$$q_b = \varepsilon_{bed} \left(\frac{\langle \Delta X \rangle - \langle \Delta z \rangle}{\Delta t} \right) \times \rho \quad (2)$$

where ε_{bed} is the volume concentration of sediment in the bed (assumed here to equal 0.35 following ref(9)), Δz is the vertical displacement associated with lee face sediment deposition (m), and ρ is the density of sediment (2,650 kg m^3). Q_b can then be defined as:

$$Q_b = \frac{\sum_{i=1}^{n} q_b}{n} \quad (3)$$

where *n* is the number of sub-sections analysed per cross-section. In order to integrate up to a channel mass flux (kg s^{-1}) across the entire channel, Q_b was multiplied by the channel width (*W*, m) obtained from the width of the bank-to-bank aDcp surveys.

To quantify bedload transport rates in the LMR, a series (*n* = 12) of repeat high-resolution bathymetric surveys of the river bed were collected at six survey areas (Fig. 1b) that permitted dune tracking between surveys to estimate channel mass bedload fluxes[27]. Surveys were conducted over the period September 2013 to July 2014 and, significantly, covered a range of flow stages (14,000 $m^3 s^{-1}$ to 55,000 $m^3 s^{-1}$, as compared to the mean peak discharge at Kratie of 36,700 $m^3 s^{-1}$ for the period 1960 – 2004[11]). Bed- and suspended- load grain size distributions were obtained during each survey (*see* Supplementary Information), whilst simultaneous flow velocity data were acquired using acoustic Doppler current profiler instruments (aDcp). The acoustic return data from the aDcp's were also used to calculate suspended sediment fluxes at each river cross-section, using previously published suspended sediment rating curves[12,31] . To construct a physically meaningful bedload transport function (Fig. 2a), we plot instantaneous bedload transport rates per unit width (kg s^{-1} m^{-1}) against excess unit stream power ($\omega - \omega_o$) following Bagnold[30], where ω is unit stream power and ω_o is critical stream power (both kg s^{-1} m^{-1}):

$$\omega = \frac{\rho g Q S}{W} \quad (1)$$

and in which ρ is the density of water (kg m^{-2}), g is the gravitational acceleration (9.81 m s^{-2}), Q is discharge (m^3 s^{-1}), S is channel slope (m m^{-1}), and W is channel width (m). The critical stream power term, ω_o, is calculated as:

$$\omega_0 = 290 D_{50}^{\frac{3}{2}} \log(12 \frac{d}{D_{50}}) \quad (2)$$

where D_{50} is the median grain size of the bed sediment (m) calculated from bed sediment samples detailed in the section above, and d is the mean flow depth (m). We integrate these unit fluxes across the channel width and assess the fraction of the total sediment flux that is composed of bedload and suspended load (as calculated from the aDcp acoustic signatures) and plot this flux against excess unit stream power (Fig. 2b). We estimate annual bedload transport rates by integrating the bedload transport function (Fig. 2a) across the time period 1980 – 2014, using flow discharge data from the Kratie gauging station (*see* Supplementary Figure S1). We subsequently estimate the proportion of sand from grain size distributions of the bed material (bedload) and suspended sediment (*see* Table S2). We note that this approach ignores any potential historical changes to bedload transport associated with the impact of basin-wide hydropower development since the completion of the first mainstem dam on the Mekong in 1993.

Non-linear regressions were then fitted between the excess stream power (see main text equations (1) and (2)) and Q_b using the Curve Fitting Toolbox in Matlab version R2014a. Specifically, a nonlinear least-squares power-law solver with one term was applied to the raw data, using the Trust-Region algorithm. The use of the power law

follows previous methods used to estimate bedload transport in a large river[30] and, although this provides a weak relationship here (r^2 = 0.22, p < 0.1), it is consistent with the statistical power of previous bedload sediment transport functions[30]. Estimates of long-term bedload flux (see Supplementary Information) were calculated using the long-term discharge and water level records from the hydrometric station at Kratie, that is operated by the Department of Hydrology and Water Resources, Cambodia, in collaboration with the Mekong River Commission (available for download from http://portal.mrcmekong.org/index). This record covers the period 1924 to 2014. To provide an appreciation of the uncertainty inherent in the bedload dataset, we use the 95% confidence bounds provided from the Matlab toolbox to bootstrap the inherent prediction uncertainty. Taking the *a* and *b* exponents of the upper and lower confidence bounds, we propagate these through the bedload transport function and excess unit stream power estimates to provide rates of bedload transport. Throughout the manuscript, our estimates are reported as the mid-point of the upper and lower 95% prediction limits plus or minus the residual to these bounds. In doing so we capture 95% of the predicted variability within our dataset.

Channel slope derivation

Channel slope was derived from single beam echo surveys of the Mekong River conducted in September 2013. Depth soundings from a Garmin Fishfinder connected to a Trimble dGPS unit, which had a positional accuracy of ~0.4 m, were adjusted for water surface slopes between gauging stations located along the Mekong River at Kratie, Kampong Cham and Neak Loeung, for the days when the

survey was conducted. The daily values were then interpolated to hourly values using a cubic spline interpolant. The water slope between the two closest gauges for each hour was calculated assuming a linear change in water slope between gauges. Distances between each gauge were calculated along the river centreline. For each hour, the water surface slope was applied to the closest gauge's water level reading to generate a variable water level for each survey date. A bathymetric surface was then generated in ArcGIS using the Topo-to-Raster toolkit at 90 m resolution. Channel slope for the survey locations shown on Figure 1 was then computed by taking the mean channel slope at each site. This coarser dataset was used as the multibeam datasets generated typically covered less than 1 km of river length, which was not sufficient to derive mean slope amongst the noise of local bedforms.

Bank Stability Analysis

The critical bank height for the onset of river bank instability under gravitational failures was estimated through a simple Culmann-type planar failure analysis[46-48] where

$$H_c = N_s\, c/\gamma \qquad (1)$$

and in which H_c is the critical bank height for the onset of mass-failure (m), c is the bank material cohesion (kN/m^2), γ is the bulk unit weight of the river bank materials (kN/m^3) and N_s is a stability number computed using:

$$N_s = (4 \sin\alpha \cos\phi)/(1 - \cos(\alpha-\phi)) \qquad (2)$$

in which α is the bank angle (degrees) and ϕ is the friction angle of the bank material (degrees).

Following Thorne et al. (1981) and Simon and Hupp (1992), we constructed river bank stability charts delineating the threshold bank height as a function of bank angle for the estimated bank material characteristics of the study reach. These bank material characteristics (bulk unit weight, alongside the cohesion and friction angle components of the material shear strength) were estimated from in-situ sampling (for bulk density and hence unit weight) and geotechnical testing (for shear strength parameters) of Lower Mekong river bank materials (Table 1). During this sampling campaign, conducted in October 2006, the shear strength parameters were estimated using an Iowa Borehole Shear Test (BST) device[47,49,50,].

Table 1: Geotechnical properties of the bank materials investigated herein

Bank material	Bulk Unit Weight (kN/m^3)	Cohesion (kN/m^2)	Friction Angle (degrees)
Silt/Clay (ML/CL)	18.831	24.7	34

To analyse river bank stability at specific locations of interest within the study reach, we plotted observed bank heights and angles, these being acquired during field surveys in October 2013 and July 2014 (19 profiles along 25 km of river bank comprised of combined terrestrial laser scanning and multibeam echo sounding; *see* above), on the stability chart. We then estimated the increase in bank height (induced by bank toe scour as a result of sand mining, either through adjacent sand mining pits or more general channel incision) required to pass the threshold bank height in order to trigger bank instability (Figure 4 in main text). The river bank

locations analysed were divided into two classes of vegetated and unvegetated banks, based on clear differences in the bank heights and angles (Figure 4 in main text) observed in the field. Note that bank material characteristics for the vegetated banks are, in our analysis, assumed to be identical to those of the unvegetated banks. In reality root reinforcement would be expected to increase the soil cohesion of the vegetated banks, but due to the difficulty in observing buried root networks it was not possible to quantify this effect in our study. This limitation does not, however, affect our overall argument because the bank stability calculations for the vegetated banks as conducted here are conservative in the sense that the vegetated banks would, in reality, be even more stable than indicated in our results.

Note that, following Thorne et al. (1981) and Simon and Hupp (1992), the critical bank height curves in the stability charts are defined for two specific conditions, referred to here as the *ambient* and/or *worst cases*. *Ambient* conditions refer to the bank material characteristics as estimated at the time of the field surveys (*i.e*., during low flow conditions), whereas *worst-case* conditions refer to a hypothetical scenario with increased bulk unit weight and reduced bank material friction angle. This hypothetical scenario is intended to represent the impacts of bank material saturation immediately following the recession of the monsoon flood. In the analysis conducted herein, the bulk unit weight for the *worst-case* scenario was increased by 10% relative to the ambient case, whereas friction angle was reduced to zero[47,48]. The ambient and worst-case curves therefore discriminate three zones on the stability charts. Specifically, the *stable* region highlights river bank morphologies that remain stable with respect to Culmann-type mass failure under both ambient and worst-case conditions, while the *permanently unstable* region discriminates bank morphologies that will be subject to Culmann-type failures, irrespective of the river bank materials

hydrological status. Finally, the *seasonally unstable* zone identifies bank morphologies that are conditionally unstable. Under ambient conditions *seasonally unstable* banks remain stable, but Culmann-type failures are anticipated at times when the bank materials become saturated, for example following the monsoon flood.

Data Availability

The raw bedload transport data collected with the multibeam echo sounder, discharge and suspended sediment data generated from the acoustic Doppler current profiler and bank profiles collected with the terrestrial laser scanner that support the findings of this study are available from the corresponding author upon reasonable request. Water discharge data used to generate the bedload ratings curves are from the hydrological records archived in the MRC data portal (http://portal. mrcmekong.org/index as discharge records from Kratie (station identifier 014901; unique data set accession 2811)).

References

1. UN. *World Urbanization Prospects 2018 - World's largest cities*. (2018).
2. Klee, H. *The Cement Sustainability Initiative Recycling Concrete*. (2009).
3. Monteiro, P. J. M., Miller, S. A. & Horvath, A. Towards sustainable concrete. *Nat. Mater.* **16,** 698–699 (2017).
4. Peduzzi, P. Sand, rarer than one thinks. *Environ. Dev.* **11,** 208–218 (2014).
5. USGS. *Mineral Commodities Summary 2015*. (2015). doi:10.3113/70140094
6. Torres, A., Brandt, J., Lear, K. & Liu, J. A looming tragedy of the sand commons. *Science (80-.).* **357,** 970–971 (2017).
7. Nittrouer, J. A. & Viparelli, E. Sand as a stable and sustainable resource for nourishing the Mississippi River delta. *Nat. Geosci.* **7,** (2014).

8. Best, J. Anthropogenic Stresses on the World ’s Big Rivers. *Nat. Geosci.* 1–59 (2018). doi:10.1038/s41561-018-0262-x

9. Bendixen, M., Best, J. L., Hackney, C. R. & Iversen, L. L. Time is running out for sand. *Nature* **571,** 29–31 (2019).

10. Milliman, J. D. & Farnsworth, K. L. *River discharge to the coastal ocean*. (2011).

11. MRC. *The Flow of the Mekong*. (2009).

12. Darby, S. E. *et al.* Fluvial sediment supply to a mega-delta reduced by shifting tropical-cyclone activity. *Nature* **539,** 276–279 (2016).

13. Walling, D. E. The changing sediment loads of the world’s rivers. *Ann. Warsaw Univ. Life Sci. – SGGW L. Reclam. NoAnn. Warsaw Univ. Life Sci. – SGGW, L. Reclam* **39,** 3–20 (2008).

14. Lu, X., Kummu, M. & Oeurng, C. Reappraisal of sediment dynamics in the Lower Mekong River, Cambodia. *Earth Surf. Process. Landforms* n/a-n/a (2014). doi:10.1002/esp.3573

15. Anthony, E. J. *et al.* Linking rapid erosion of the Mekong River delta to human activities. *Nat. Publ. Gr.* (2015). doi:10.1038/srep14745

16. Kondolf, G. M., Rubin, Z. K. & Minear, J. T. Dams on the Mekong: Cumulative sediment starvation. *Water Resour. Res.* **50,** 5158–5169 (2014).

17. Koehnken, L. *IKMP Discharge and Sediment Monitoring Programme Review, Recommendations and Data Analysis, Parts 1 & 2.* (2012).

18. Schmitt, R. J. P., Rubin, Z. & Kondolf, G. M. Losing ground - scenarios of land loss as consequence of shifting sediment budgets in the Mekong Delta. (2017). doi:10.1016/j.geomorph.2017.04.029

19. Kondolf, G. M. *et al.* Changing sediment budget of the Mekong: Cumulative

threats and management strategies for a large river basin. *Sci. Total Environ.* **625,** 114–134 (2018).

20. Cochrane, T. A., Arias, M. E. & Piman, T. Historical impact of water infrastructure on water levels of the Mekong River and the Tonle Sap system. *Hydrol. Earth Syst. Sci.* **18,** 4529–4541 (2014).
21. Räsänen, T. A. *et al.* Observed river discharge changes due to hydropower operations in the Upper Mekong Basin. *J. Hydrol.* **545,** 28–41 (2017).
22. Bravard, J.-P. & Goichot, M. Geography of sand and gravel mining in the Lower Mekong River. *EchoGéo* **26,** (2013).
23. Brunier, G., Anthony, E. J., Goichot, M., Provansal, M. & Dussouillez, P. Recent morphological changes in the Mekong and Bassac river channels, Mekong delta: The marked impact of river-bed mining and implications for delta destabilisation. *Geomorphology* **224,** 177–191 (2014).
24. Barman, B., Kumar, B. & Sarma, A. K. Turbulent flow structures and geomorphic characteristics of a mining affected alluvial channel. *Earth Surf. Process. Landforms* **43,** 1811–1824 (2018).
25. Kondolf, G. M. Hungry water: Effects of dams and gravel mining on river channels. *Environ. Manage.* **21,** 533–551 (1997).
26. Ashraf, M. A., Maah, M. J., Yusoff, I., Wajid, A. & Mahmood, K. Sand mining effects, causes and concerns: A case study from Bestari Jaya, Selangor, Peninsular Malaysia. *Sci. Res. Essays* **6,** 1216–1231 (2011).
27. Nittrouer, J. A., Allison, M. A. & Campanella, R. Bedform transport rates for the lowermost Mississippi River. *J. Geophys. Res. Earth Surf.* **113,** 1–16 (2008).
28. Turowski, J. M., Rickenmann, D. & Dadson, S. J. The partitioning of the total sediment load of a river into suspended load and bedload: a review of

empirical data. *Sedimentology* **57,** 1126–1146 (2010).

29. Koehnken, L. *The ISH 0306 Study Development of Guidelines for Hydropower Environmental Impact Mitigation and Risk Management in the Lower Mekong Mainstream and Tributaries Hydropower Risks and Impact Mitigation Guidelines and Recommendations*. (2014).
30. Bagnold, R. A. An Empirical Correlation of Bedload Transport Rates in Flumes and Natural Rivers. *Proc. R. Soc. A Math. Phys. Eng. Sci.* **372,** 453–473 (1980).
31. Hackney, C. R. *et al.* The influence of flow discharge variations on the morphodynamics of a diffluence-confluence unit on a large river. *Earth Surf. Process. Landforms* (2017). doi:10.1002/esp.4204
32. Bravard, J.-P., Goichot, M. & Tronchère, H. An assessment of sediment-transport processes in the Lower Mekong River based on deposit grain sizes, the CM technique and flow-energy data. *Geomorphology* (2013). doi:10.1016/j.geomorph.2013.11.004
33. Kazuaki, H., Shigeko, H. & Sieng, S. Sedimentary Facies of Borehole Cores from the Mekong River Floodplain in Cambodia. *Geogr. Rev. Jpn.* **80,** 681–692 (2007).
34. Tamura, T. *et al.* Depositional facies and radiocarbon ages of a drill core from the Mekong River lowland near Phnom Penh, Cambodia: Evidence for tidal sedimentation at the time of Holocene maximum flooding. *J. Asian Earth Sci.* **29,** 585–592 (2007).
35. Kubo, S. Geomorphological features and subsurface geology of the Lower Mekong Plain around Phnom Penh City, Cambodia (South East Asia). *Rev. Geogr. Acad.* **2,** 20–32 (2008).

36. Tamura, T. *et al.* Initiation of the Mekong River delta at 8 ka: evidence from the sedimentary succession in the Cambodian lowland. *Quat. Sci. Rev.* **28,** 327–344 (2009).

37. Nguyen, V. L., Ta, T. K. O. & Saito, Y. Early Holocene initiation of the Mekong River delta, Vietnam, and the response to Holocene sea-level changes detected from DT1 core analyses. *Sediment. Geol.* **230,** 146–155 (2010).

38. Liu, P. *et al.* Stratigraphic Formation of the Mekong River Delta and Its Recent Shoreline Changes. *Oceanography* **30,** 72–83 (2017).

39. Uhlemann, S., Kuras, O., Richards, L. A., Naden, E. & Polya, D. A. Electrical resistivity tomography determines the spatial distribution of clay layer thickness and aquifer vulnerability, Kandal Province, Cambodia. *J. Asian Earth Sci.* **147,** 402–414 (2017).

40. Szupiany, R. N., Amsler, M. L., Best, J. L. & Parsons, D. R. Comparison of Fixed- and Moving-Vessel Flow Measurements with an aDp in a Large River. J. Hydrol. Eng. 133, 1299–1309 (2007).

41. Parsons, D. R. R. et al. Velocity Mapping Toolbox (VMT): a processing and visualization suite for moving-vessel ADCP measurements. Earth Surf. Process. Landforms 38, 1244–1260 (2013).

42. Lane, S. N., Bradbrook, K. F., Richards, K. S., Biron, P. M. & Roy, A. G. Secondary circulation cells in river channel confluences : measurement artefacts or coherent flow structures ? Hydrol. Process. 14, 2047–2071 (2000).

43. Kostaschuk, R., Best, J., Villard, P., Peakall, J. & Franklin, M. Measuring flow velocity and sediment transport with an acoustic Doppler current profiler. Geomorphology 68, 25–37 (2005).

44. Szupiany, R. N., Amsler, M. L., Parsons, D. R. & Best, J. L. Morphology, flow structure, and suspended bed sediment transport at two large braid-bar confluences. Water Resour. Res. 45, n/a-n/a (2009).

45. Shugar, D. H. et al. On the relationship between flow and suspended sediment transport over the crest of a sand dune, Río Paraná, Argentina. Sedimentology

46. Carson, M.A. and Kirkby, M.J. 1972. Hillslope Form and Process, Cambridge University Press, London.

47. Thorne, C.R., Murphey, J.B. and Little, W.C. 1981. Stream channel stability, Appendix D, Bank stability and bank material properties in the bluffline streams of northwest Mississippi, US Department of Agriculture, National Sedimentation Laboratory, Oxford, Mississippi.

48. Simon, A. and Hupp, C.R. 1992. Geomorphic and vegetative recovery processes along modified stream channels of West Tennessee, US Geological Survey, Open-File Report 91-502, Nashville, Tennessee.

49. Handy, R.L. and Fox, J.S. 1967. A soil borehole direct-shear test device. Highway Research News, 27, 42-51.

50. Lohnes, R.A. and Handy, R.L. 1968. Slope angles in friable loess. Journal of Geology, 76(3), 247-258.

Figure Captions

Figure 1: Sediment dynamics of the Mekong River. a, Sediment extraction rates (Mt yr^{-1}) across the Mekong River basin with the composition of the extracted load depicted in the pie charts (from Bravard et al., 2013). The size of the pie charts scales with the volume of sediment extracted. The national boundary of Cambodia is shown and highlights the location of panel **b**. The location of the previous bedload transport estimate for the LMR is highlighted at Kratie, Cambodia. **b,** Locations of multibeam echo sounder surveys (stars) used herein to estimate bedload transport rates. Histograms show the instantaneous sand fluxes in suspension at each cross-section during each survey period. Pie charts denote the average composition of sediment in grain size fractions at each survey location. Base map credit: Esri, DeLorme Publishing Company, Inc.

Figure 2: Bedload transport functions for the Mekong River. a, Relationship between bedload transport rate per unit width (q_b) and excess unit stream power (ω-ω_0) (r^2 = 0.22 n = 12, P = 0.002). Dashed lines represent the 95% confidence bounds. **b**, Relationship between the percentage of the total sediment flux that is bedload ($Q_{b\%}$) and excess unit stream power (ω-ω_0) (r^2 = 0.36 n = 12, P = 0.003). **c**. Daily bedload flux (Q_b; Mt day^{-1}) for the period 1981 – 2014. The cyan shaded area depicts the range of bedload transport rates captured by our surveys. Integrating bedload fluxes over the 34 year period for the range highlighted by the cyan box reveals that our surveys capture 78% of all bedload transport during this period.

Flows lower than 14,000 m^3 s^{-1} account for 19% of bedload transport, whilst flows higher than 55,000 m^3 s^{-1} account for just 3% of the long-term bedload flux.

Figure 3: Morphological impacts of sand mining on river bathymetry. a. MBES bathymetric map (July, 2014) of the Mekong River at Phnom Penh, Cambodia, with elevations relative to mean sea-level as defined by the EGM08 geoid. Deep pockmarks can be seen in this area. Flow is from bottom to top. **b.** The relationship between mining pit depth and pit diameter from pits identified in **a** (n = 559; p < 0.05). Histograms showing the distributions of the depths and diameters of the pits are provided.

Figure 4: a, Image of properties affected by bank collapses on the Mekong River, Cambodia. **b,** Bank stability diagram populated with bank height and angle data derived from terrestrial laser scanner and MBES data for 19 bank profiles along 25 kilometres of Mekong River banks in Cambodia. Shaded vertical bars depict how incremental lowering of the bed (of up to six meters, based on the distribution of pit depths depicted in Figure 3b) increases bank height from the current bed level. Green-scale bars depict banks covered in vegetation whilst grey-scaled bars are unvegetated bank profiles. **c,** Bar charts for unvegetated, vegetated and combined bank profiles, highlighting the shift in bank stability from stable to seasonally unstable conditions as the river bed is lowered.

Fig 1

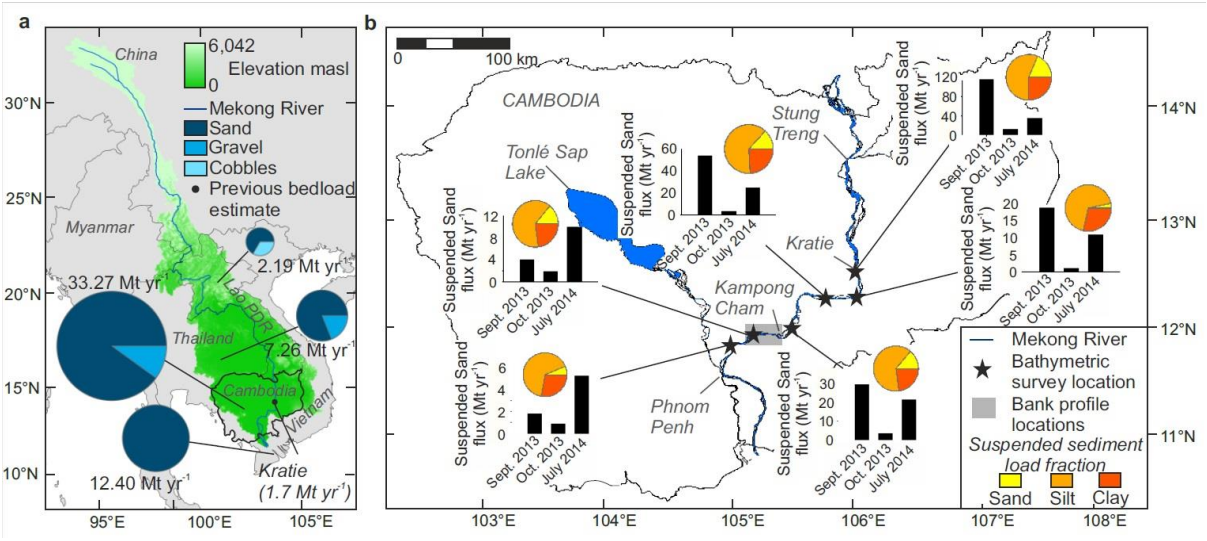
a
b
China
Myanmar
Thailand
Lao PDR
Cambodia
Vietnam
6,042
0
Elevation masl
Mekong River
Sand
Gravel
Cobbles
Previous bedload estimate
33.27 Mt yr-1
2.19 Mt yr-1
7.26 Mt yr-1
12.40 Mt yr-1
Kratie
(1.7 Mt yr-1)
95°E
100°E
105°E
30°N
25°N
20°N
15°N
10°N
0
100 km
CAMBODIA
Tonlé Sap Lake
Stung Treng
Kratie
Kampong Cham
Phnom Penh
Suspended Sand flux (Mt yr-1)
Sept. 2013
Oct. 2013
July 2014
103°E
104°E
105°E
106°E
107°E
108°E
14°N
13°N
12°N
11°N
Mekong River
Bathymetric survey location
Bank profile locations
Suspended sediment load fraction
Sand
Silt
Clay

Fig 2

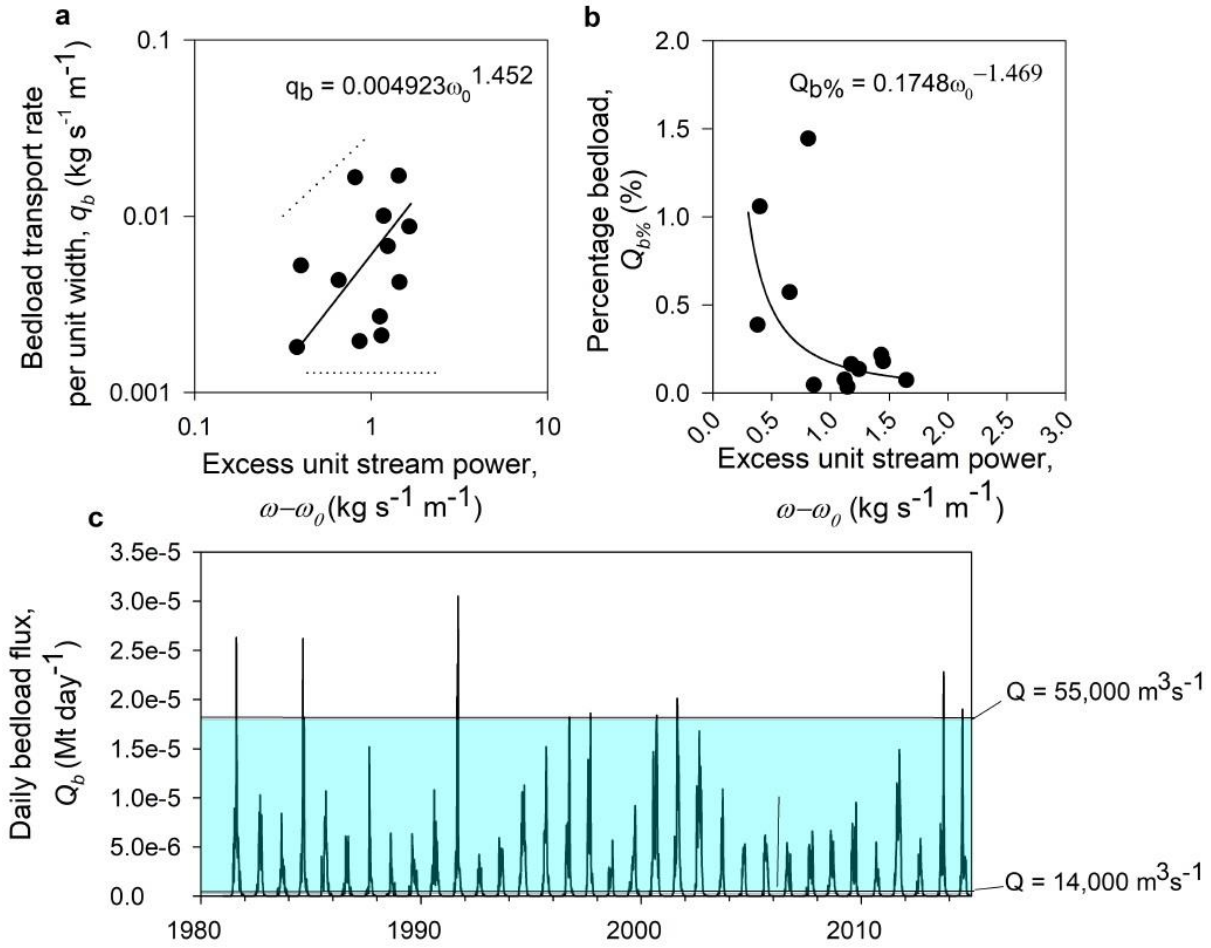
a
Bedload transport rate per unit width, q_b (kg s^{-1} m^{-1})
$q_b = 0.004923\omega_0^{1.452}$
Excess unit stream power, $\omega-\omega_0$ (kg s^{-1} m^{-1})
b
Percentage bedload, $Q_{b\%}$ (%)
$Q_{b\%} = 0.1748\omega_0^{-1.469}$
Excess unit stream power, $\omega-\omega_0$ (kg s^{-1} m^{-1})
c
Daily bedload flux, Q_b (Mt day^{-1})
Q = 55,000 m^{3}s^{-1}
Q = 14,000 m^{3}s^{-1}

Fig 3

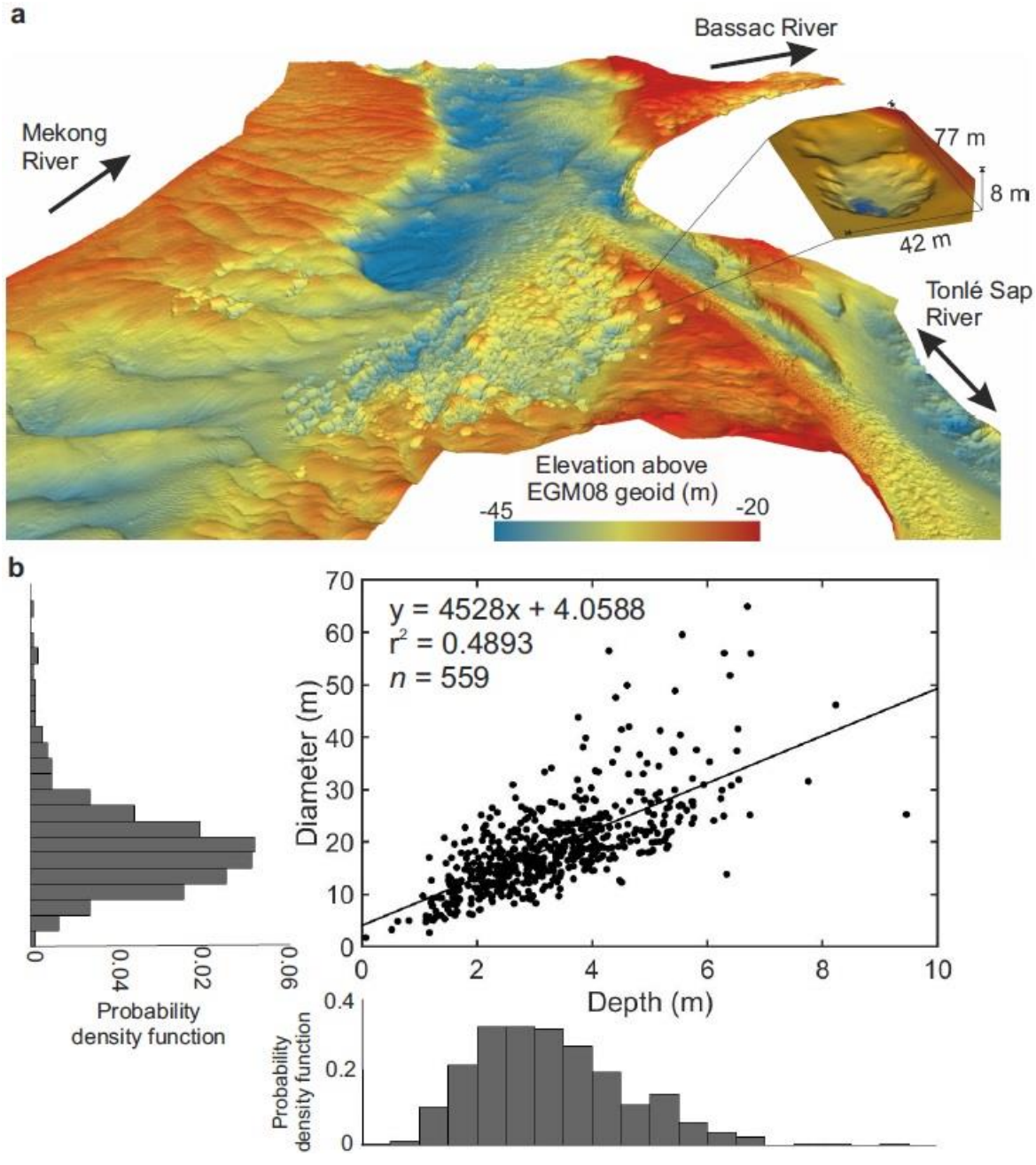
a
Bassac River
Mekong River
77 m
8 m
42 m
Tonlé Sap River
Elevation above EGM08 geoid (m)
-45
-20
b
y = 4528x + 4.0588
r² = 0.4893
n = 559
Diameter (m)
Depth (m)
Probability density function
Probability density function

Fig 4

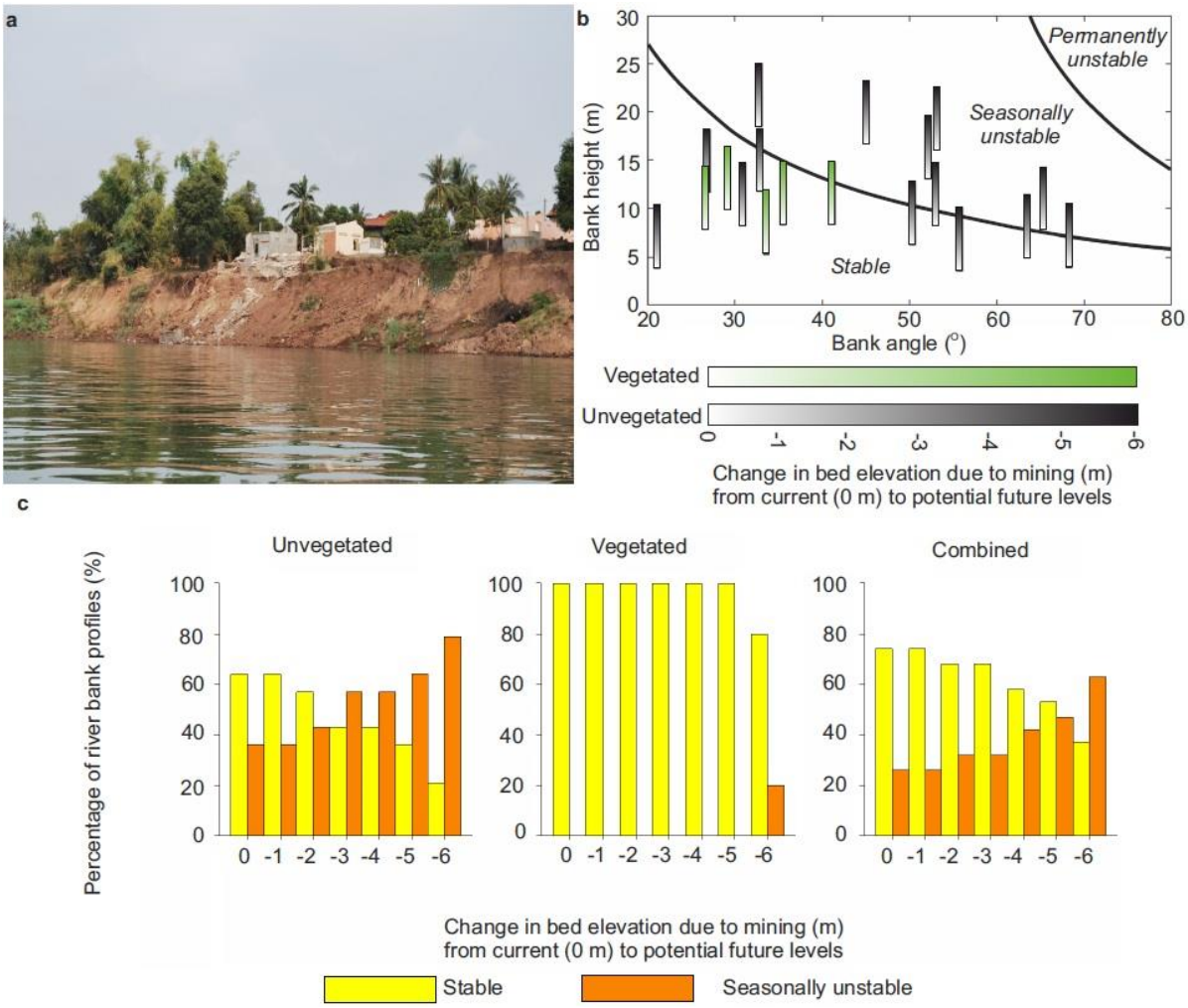
a
b
Permanently unstable
Seasonally unstable
Stable
Bank height (m)
Bank angle (°)
Vegetated
Unvegetated
Change in bed elevation due to mining (m) from current (0 m) to potential future levels
c
Unvegetated
Vegetated
Combined
Percentage of river bank profiles (%)
Change in bed elevation due to mining (m) from current (0 m) to potential future levels
Stable
Seasonally unstable

Supplementary Information

River bank instability from unsustainable sand mining in the lower Mekong River

Christopher R. Hackney[1]*, Stephen E. Darby[2], Daniel R. Parsons[1], Julian Leyland[2], James L. Best[3], Rolf Aalto[4], Andrew P. Nicholas[4] and Robert C. Houseago[1].

[1]Energy and Environment Institute, University of Hull, Hull, HU6 7RX, UK

[2]School of Geography and Environmental Sciences, University of Southampton, Southampton, SO17 1BJ, UK.

[3]Departments of Geology, Geography and GIS, Mechanical Science and Engineering and Ven Te Chow Hydrosystems Laboratory, University of Illinois at Urbana-Champaign, Urbana, IL 61801, USA.

[4]College of Life and Environmental Sciences, University of Exeter, Exeter, EX4 4RJ, UK.

**Corresponding author email address: c.hackney@hull.ac.uk; (https://orcid.org/0000-0001-5390-9136)*

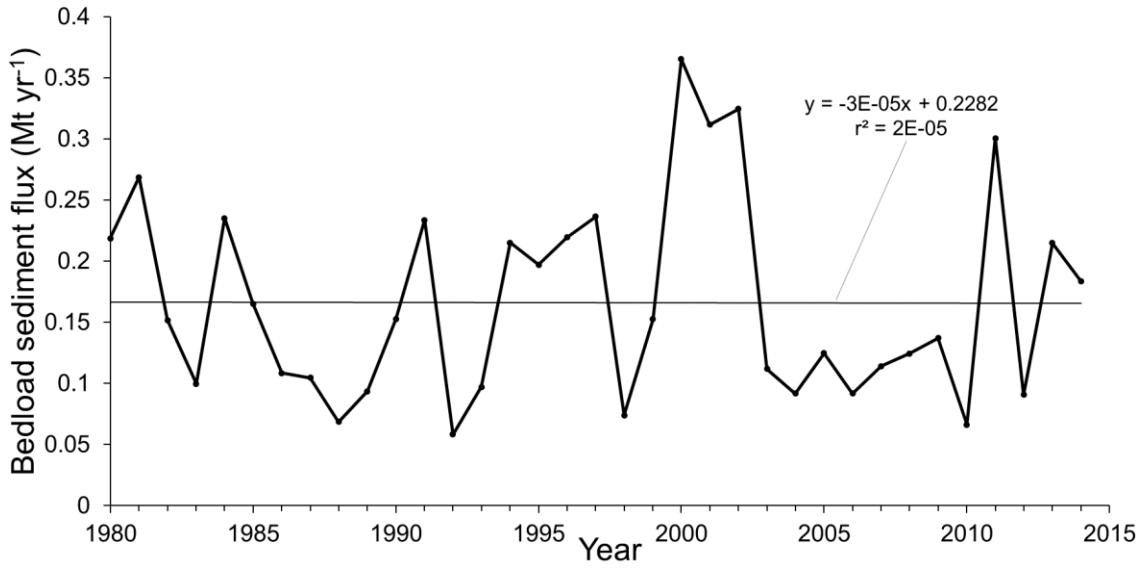

Supplementary Figure 5: Long term trends in annualised bedload sediment flux (Mt yr^{-1}) over the period 1980 to 2014 estimated using the historic discharge record from Kratie, Cambodia, highlighting the long term linear trend in bedload sediment flux.

Supplementary Table 1: Site characteristics for survey locations

Date	Survey Site ID	Lat	Long	Q (m3 s^{-1})	Max depth (m)	Mean depth (m)	Mean cross-section velocity (m s^{-1})	Channel Mass Flux (Kg/s)
Sept 2013	1	11.81287	104.99137	25000	42.3	21.6	1.25	1.458
Sept 2013	2	11.94926	105.19539	27000	42.1	20.2	1.22	3.790
Sept 2013	3	12.26019	105.80312	30000	29.7	23.1	1.15	2.374
Sept 2013	4	12.26019	105.80312	49000	20.4	16.6	1.65	28.201
Sept 2013	5	12.26152	105.98770	55000	29.4	21.9	2.14	14.232
Oct 2013	2	11.94926	105.19539	15500	40.1	13.3	0.79	14.909
Oct 2013	3	12.26019	105.80312	14500	27.5	20.1	0.70	4.529
Oct 2013	4	12.26019	105.80312	14400	13.5	10.4	0.58	8.723
Oct 2013	5	12.26152	105.98770	14000	21.2	11.4	0.59	2.939
July 2014	2	11.94926	105.19539	27000	40.3	20.1	1.11	7.145
July 2014	4	12.26152	105.98770	29000	17.7	13.0	1.30	3.179
July 2014	6	12.46544	106.01929	34000	22.5	15.0	1.58	14.046

***Supplementary Table* 2:** Median grain size and percentage sand, silt and clay of bed material and suspended load for the six sites surveyed.

Survey Site	***Lat.***	***Long.***	***Bedload***	***Suspended Sediment***		
			D_{50} (µm)	**%Sand**	**%Silt**	**%Clay**
1	11.81287	104.99137	350	3	62	34
2	11.94926	105.19539	366	6	66	28
3	11.89619	105.39720	211	14	63	23
4	12.26019	105.80312	352	13	63	24
5	12.26152	105.98770	383	5	63	29
6	12.46544	106.01929	500	19	56	25

***Supplementary Table 3*:** Estimates of the depth of sand deposits across the Lower Mekong Basin in Cambodia and Vietnam.

Lat	***Lon***	***Location***	***Depth of bedrock***	***Sand deposit thickness***	***Description***	***Citation***
Unreported	*Unreported*	Kampong Cham Bridge		44.5 m	Borehole	Kubo (2008)
Unreported	*Unreported*	National Road 6A Bridge	27 m		Borehole	Kubo (2008)
Unreported	*Unreported*	National Road 6A upstream of 2.	29.5 m	9 m	Borehole	Kubo (2008)
Unreported	*Unreported*	Prek Tnaot	36.5 m	21 m	Borehole	Kubo (2008)
Unreported	*Unreported*	Chroy Chang Var Bridge	17.4 m	>9 m	Borehole	Kubo (2008)
Unreported	*Unreported*	Phnom Penh (SE)	>37 m		Borehole	Kubo (2008)
Unreported	*Unreported*	Kandal Province		>100 m	Borehole	Kubo (2008)
11°43.833" N	*104° 57.85' E*	End of abandoned channel on Mekong River west bank	> 25 m		Core	Kazukai et al. (2007)
11°43.833" N	*104° 57.75' E*	East bank of the Bassac River	> 10.5 m	> 6m	Core	Kazukai et al. (2007)
12°00.983" N	*104° 46.033' E*	Floodplain on west bank of the Tonlé Sap River	> 7m	1 m	Core	Kazukai et al. (2007)
11°43.833" N *11°28.823"N* *12°00'983"N*	*104°57.85" E* *104°57.75" E* *104°46.033' E*	Several cores and boreholes through the Mekong delta	38 – 52 m	24 - 42 m	Borehole	Kazukai et al. (2007)
11°28.829' N	*105° 07.207' E*		> 30.5 m	0	Core	Tamura et al. (2009)

11° 11.547′ N	*105° 16.638′ E*	Natural levee east bank of Mekong River 20 km SE of PP		0	Core	Tamura et al. (2009)
11°57.558′ N	*105° 03.613′ E*	Floodplain on west bank of the Bassac River		0	Core	Tamura et al. (2009)
11°28.2′ N	*105° 07.8′ E*	20 km southeast of PP in Kean Svay District (floodplain)	>31 m	17 m	Core	Tamura et al. (2007)
Unreported	*Unreported*	CHIRP seismic data from Mekong delta offshore		22m	Core	Liu et al. (2017)
11°27.023'N	*105°05.149'E*	Aquifer thickness estimated from resistivity surveys between the Mekong and Bassac river channels		>25 m	Resistivity measurements	Uhlemann et al. (2017)

References

Kazuaki, H., Shigeko, H. & Sieng, S. Sedimentary Facies of Borehole Cores from the Mekong River Floodplain in Cambodia. *Geogr. Rev. Jpn.* **80,** 681–692 (2007).

Kubo, S. Geomorphological features and subsurface geology of the Lower Mekong Plain around Phnom Penh City, Cambodia (South East Asia). *Rev. Geogr. Acad.* **2,** 20–32 (2008).

Liu, P. *et al.* Stratigraphic Formation of the Mekong River Delta and Its Recent Shoreline Changes. *Oceanography* **30,** 72–83 (2017).

Tamura, T. *et al.* Depositional facies and radiocarbon ages of a drill core from the Mekong River lowland near Phnom Penh, Cambodia: Evidence for tidal sedimentation at the time of Holocene maximum flooding. *J. Asian Earth Sci.* **29,** 585–592 (2007).

Tamura, T. *et al.* Initiation of the Mekong River delta at 8 ka: evidence from the sedimentary succession in the Cambodian lowland. *Quat. Sci. Rev.* **28,** 327–344 (2009).

Uhlemann, S., Kuras, O., Richards, L. A., Naden, E. & Polya, D. A. Electrical resistivity tomography determines the spatial distribution of clay layer thickness and aquifer vulnerability, Kandal Province, Cambodia. *J. Asian Earth Sci.* **147,** 402–414 (2017).